LDA+U calculation of electronic and thermoelectric properties of doped $CuCoO_2$

K. Knížek
Institute of Physics ASCR, Cukrovarnická 10, 162 00 Prague 6, Czech Republic
(Received 6 January 2015; published 23 February 2015)

Doped $CuCoO_2$ is a candidate oxide material for thermoelectric power generation. The evolution of the band structure and thermoelectric properties of $CuCoO_2$ upon hole and electron doping in the CoO_2 layer and hole doping at the Cu site were calculated by the local-density approximation (LDA) and LDA+U methods and using standard Boltzmann theory. The doping was simulated by the virtual atom approximation and the supercell approach and the results were compared with previous calculations using the rigid band approximation. The calculated thermopowers are comparable for the virtual atom and rigid band approximations, but the thermopower obtained from the supercell calculation is significantly lower. The reason is the similar energy of Co and Cu d orbitals and the hybridization of symmetrically related Co a_{1g} and Cu d_{z^2} orbitals. As a consequence, both cations contribute to the bands around the Fermi level and hence a substitution at any of the cation sites alters the band structure at E_F and affects the thermoelectric properties. Our results show that in the case of hole doping, higher thermopower is obtained for substitution at the Cu site than in the CoO_2 layer.

DOI: 10.1103/PhysRevB.91.075125 PACS number(s): 71.15.Mb, 72.20.Pa, 84.60.Rb

I. INTRODUCTION

In the family of layered systems, the oxides comprising the two-dimensional triangular network of transition-metal cations have attracted a lot of interest in fundamental and applied research. Among them, delafossites exhibit a wide range of possible applications, such as superconductors, giant/colossal magnetoresistance materials, and transparent conducting oxides.

Delafossite oxides have a general chemical formula, ABO_2, where the B cation is in the center of a trigonally distorted octahedra, forming hexagonal BO_2 sheets, and the A cation is linearly coordinated between them. Whereas the B cation is usually in a trivalent state and can be almost any transition metal, the choice of the A cation is more limited due to the requirement of a monovalent state and stability in linear coordination. Typical examples of A cations are Cu, Ag, Pd, and Pt. The symmetry of the structure is either rhombohedral (space group $R\bar{3}m$) or hexagonal (space group $P6_3/mmc$).

Structurally related Na_xCoO_2 cobaltates, where Na is in prismatic or octahedral coordination instead of linear, are promising p-type electronic materials for thermoelectric applications as they combine an extraordinary high Seebeck coefficient with metalliclike conductivity [1–3]. One of the important advantages of Na_xCoO_2 and other oxide thermoelectric materials is a natural stability in an ambient oxidative environment. However, the performance of Na_xCoO_2 is still inferior compared to classical thermoelectric materials such as Bi_2Te_3; see, e.g., the review in Ref. [4]. In addition, a low resistance of Na_xCoO_2 to humidity, which was experimentally evidenced in Ref. [5], also limits the range of applications of this material. Another problem which complicates the application of cobaltates is that all of them are only p type, and other materials such as doped $SrTiO_3$ and $CaMnO_3$ should be used as n type. Since different types of materials exhibit different mechanical properties, namely, thermal dilatation, the combination of these materials in one thermoelectric module is more complicated than a fabrication of the module consisting of one type of material that can be doped both to p and n type. Thus the investigation of oxide material with the possibility of doping by electron and holes is highly desirable. Recently, it has been suggested, based on local-density approximation (LDA) calculations and a rigid band approximation, that a doped $CuCoO_2$ might also be a suitable candidate oxide material for thermoelectric power generation [6].

$CuCoO_2$ crystallizes in a rhombohedral structure, space group $R\bar{3}m$. The occupied Wyckoff positions are Cu in $3a(0,0,0)$, Co in $3b(0,0,1/2)$, and O in $6c(0,0,z)$, with $z = 0.111$ [7]. The synthesis of this compound is not straightforward. $CuCoO_2$ has been mainly prepared by an ion-exchange method [8–10]; however, other synthesis routes such as solution-based techniques [11], thermal decomposition of hydroxysalts [12], and hydrothermal synthesis [13] were used. As regards transport and magnetic properties, $CuCoO_2$ is a nonmagnetic insulator, in agreement with formal charge assignments of Cu^{1+} and Co^{3+} for the transition-metal constituents. Transport properties are governed by the overlap of transition-metal d orbitals with oxygen p orbitals, that depend on the relative position of d orbitals on the energy scale, which is determined by the crystal field of the corresponding coordination. The Co^{3+} d orbitals split in the crystal field of trigonal coordination compressed along the z axis into orbitals e_g, a_{1g}, and e'_g, and Cu^{1+} d orbitals in the crystal field of linear coordination into orbitals d_{z^2}, $d_{xz} + d_{yz}$, and $d_{x^2-y^2} + d_{xy}$; see Fig. 1.

The electronic structure of $CuCoO_2$ calculated in Ref. [6] evidences similarities with thermoelectric Na_xCoO_2, although it is much less two dimensional. The obtained valence-band dispersion was used for calculations of the Seebeck coefficients within Boltzmann transport equations (BOLTZTRAP package [14]) and the results showed high thermopower comparable to Na_xCoO_2.

The actual successful doping at the B site is conditioned by the existence of an isostructural compound with a transition-metal adjacent in the periodic table, i.e., $CuFeO_2$ concerning hole doping and $CuNiO_2$ for electron doping. $CuFeO_2$ indeed crystallizes in the same symmetry $R\bar{3}m$ [15,16]. As regards transport properties of $CuFeO_2$, electrical resistivity exhibits a typical temperature dependence of a semiconductor, and thermopower is high and positive around 400 μV/K above room

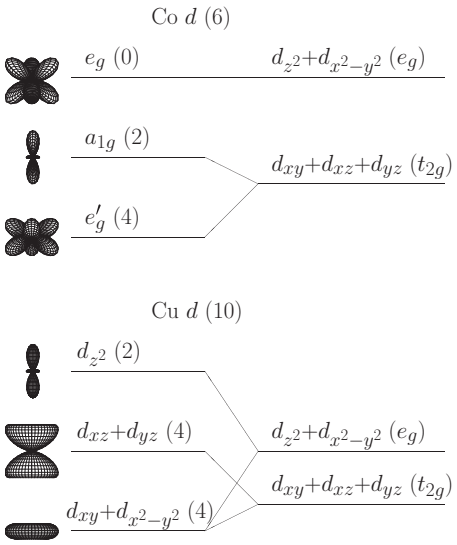

FIG. 1. Splitting of Co d orbitals in a crystal field of trigonally distorted octahedral coordination and Cu d orbitals in linear coordination, in comparison with splitting in a crystal field of regular octahedra. The ideal orbital occupations are in parentheses. The orbitals that point toward the bonding oxygens, i.e., Co e_g and Cu d_{z^2}, have the highest energy in the one-electron approximation.

temperature [17]. Geometrically frustrated antiferromagnetic ordering in a triangular lattice with spin moment pointing along the c axis is formed at low temperature after crossing two successive magnetic transitions at $T_{N1} = 16$ K and $T_{N2} = 11$ K [16,18,19]. $CuNiO_2$ was not synthesized so far, but there exist delafossites where Ni is mixed with another cation in the B site, e.g., $CuNi_{1/3}V_{2/3}O_2$ [20], the existence of which is probably enabled by a charge disproportionation $CuNi^{2+}_{1/3}V^{3+}_{1/3}V^{4+}_{1/3}O_2$. In this context, a partial Ni doping for Co would be plausible.

An additional possibility of altering the carrier concentration is a doping at the A site. However, since Cu^+ has the electron configuration d^{10}, the hole doping could only be considered, namely, replacing Cu^+ by Ni^+. In addition, it must be taken into account that Ni is not likely to accept 1+ valence and to occur in linear coordination. Therefore, the Ni substitution will only be used in the virtual atom approximation, since this approximation is only defined for two atoms adjacent in the periodic table. In the supercell calculation, the actual substitution will be realized with Pd^+ because the $PdCoO_2$ phase exists and is isostructural with $CuCoO_2$ adopting $R\bar{3}m$ symmetry. In contrast to $CuCoO_2$, electrical conductivity of $PdCoO_2$ is metallic and highly anisotropic, and thermopower is positive and as low as 2–4 μV/K [21,22]. Electronic structure calculations revealed that overlaps between hybrid orbitals composed of Pd $4d_{z^2}$, $4d_{x^2-y^2}$, and $4d_{xy}$ at the Fermi level result in delocalized metallic bonding and are responsible for the high electrical conductivity, whereas CoO_2 layers are rather insulating [23,24].

For the sake of completeness, we should also mention the possibility of doping by varying oxygen stoichiometry. However, we expect that this kind of phase would be unstable against the tendency to attain the ideal stoichiometry at high temperature in an ambient atmosphere, so it will not be considered in this work.

The aim of this work is the investigation of the electronic structure of $CuCoO_2$ doped by holes and electrons using the virtual atom (VA) approximation and supercell calculation. Doping at both A and B sites will be considered. The VA is realized by averaging the number of electrons and atom number of two atoms adjacent in the periodic table, namely, $Co_{1-x}Fe_x$ and $Co_{1-x}Ni_x$ for the B site and $Cu_{1-x}Ni_x$ for the A site. In the supercell calculation, Fe and Ni will be partially substituted at the B site, but Pd instead of Ni will be used for hole doping in the A site.

Finally, the data on the valence-band dispersion will be used for calculations of the Seebeck coefficients within Boltzmann transport equations (BOLTZTRAP package [14]) and results for various doping approximations, i.e., the rigid band approximation, virtual atom approximation, and supercell calculation, will be confronted.

II. METHODS OF CALCULATIONS

The calculations were made with the WIEN2K program [25]. This program is based on the density functional theory (DFT) and uses the full-potential linearized augmented plane-wave (FP LAPW) method with the dual basis set. In the LAPW methods, the space is divided into atomic spheres and the interstitial region. The electron states are then classified as the core states that are fully contained in the atomic spheres and the valence states. The valence states are expanded using the basis functions; each of the basis functions has the form of the plane wave in the interstitial region, while it is an atomiclike function in the atom spheres.

Calculations using the virtual atom approximation were done in the $R\bar{3}m$ cell containing three formula units. The supercell calculations were done in a 4× enlarged cell containing 12 formula units and defined by $\vec{a_S} = 2\vec{a}$, $\vec{b_S} = \vec{a} + 2\vec{b}$, and $\vec{c_S} = \vec{c}$.

The core states were defined as an electronic configuration (Ne $3s^2$) for Fe, Co, Ni, and Cu, as Ar $3d^{10}$ $4s^2$ for Pd, and as He for O atoms. The radii of the atomic spheres were taken 2.0 a.u. for transition-metal atoms and 1.55 a.u. for O. The number of k points in the irreducible part of the Brillouin zone was 110 for the $R\bar{3}m$ cell and 42 for the supercell. All calculations were spin polarized.

To improve the description of $3d$ electrons, we used the LDA+U method. In this method, an orbitally dependent potential is introduced for the chosen set of electron states, i.e., for $3d$ states. This additional potential has an atomic Hartree-Fock form, but with screened Coulomb and exchange interaction parameters. The fully localized limit version of the LDA+U method was employed. The value $U = 2.7$ eV was used, which is the same as for the $LaCoO_3$ compound in [26,27]. The aim was to investigate the trend introduced by correlation effects. The determination of the appropriate values of U is beyond the scope of this paper.

The calculation of the Seebeck coefficients was done within Boltzmann transport theory using the BOLTZTRAP package [14] under the constant relaxation-time approximation for the charge carriers.

III. RESULTS AND DISCUSSION

The calculated density of states (DOS) of $CuCoO_2$ using LDA and LDA+U are displayed in Fig. 2. The character of the DOS obtained by LDA calculations is insulating with a gap of about 0.6 eV. The states within the range 0–1 eV below E_F are formed by Co d bands and within the range 1–3 eV by Cu d bands. The oxygen bands start to prevail below 3 eV. The ideal occupation of d orbitals for expected valencies Cu^+ is d^{10}, and Co^{3+} in the low-spin (LS) state is d^6. However, the pronounced hybridization with oxygen p bands results in deviation of the calculated occupations from the ideal values, so that the occupation of Co d orbitals is increased to 6.7 electrons. Similar value 6.6 electrons of Co d orbital occupation were found, e.g., in typical cobalt perovskite $LaCoO_3$ with Co^{3+} in a low-spin state [26].

Let us note that in the DFT method, the occupation of orbitals is actually counted inside the spheres, excluding interstitial electrons, so it should not be interpreted as an indication of a valence state. A suitable method to quantify the atomic charges is, e.g., the atoms in molecule (AIM) concept of Bader [28]. The advantage of this method is that the analysis is based solely on the charge density, so it is independent of the basis set and atomic spheres used. Using this method, it was proven that 95% of interstitial electrons are associated with oxygen atoms in typical transition-metal oxides; see, e.g., [29]. Thus the occupation of d orbitals inside the spheres is very close to their total occupation.

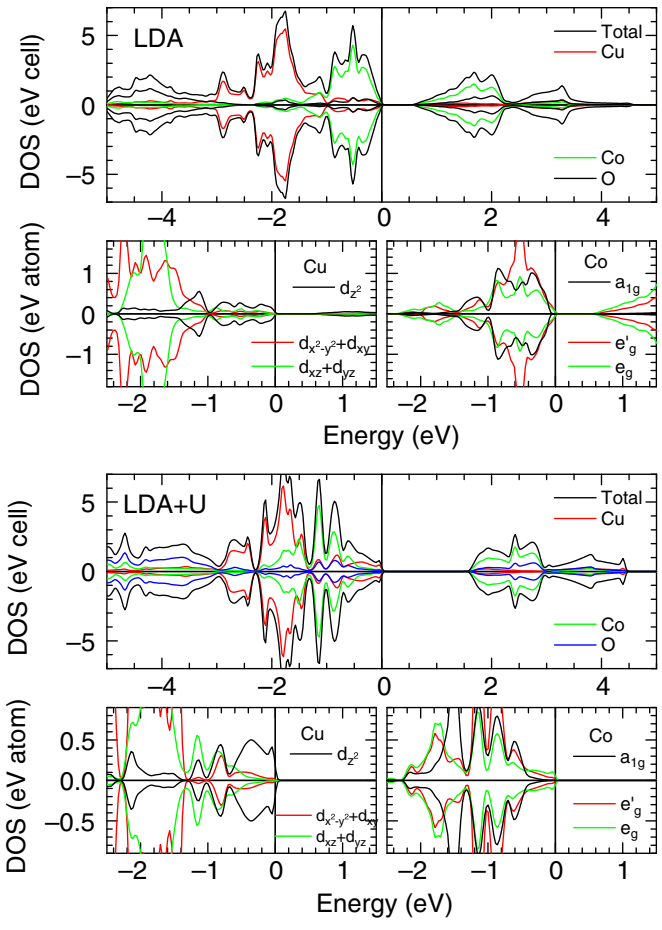

FIG. 2. (Color online) LDA (upper panels) and LDA+U (lower panels) density of states, and projections of Cu and Co d orbitals onto LAPW spheres, for $CuCoO_2$. The total DOS is *per* primitive unit cell, and the partial DOS is *per* atom.

An additional effect of the transition-metal d orbitals and oxygen p-orbital hybridization is widening and consequently overlapping of the d bands. Thus the occupation of d orbitals split by a trigonal field (see Fig. 1), which is for low-spin Co^{3+} in the ideal case $e'^4_g\ a^2_{1g}\ e^0_g$, is changed to $e'^{2.8}_g\ a^{1.8}_{1g}\ e^{2.1}_g$ occupations in the LDA calculation. Moreover, the character of Co d bands near the Fermi level is a mixture of e'_g and e_g, whereas the bands of a_{1g} symmetry, which should be the nearest to E_F according to ideal splitting of orbitals in a trigonal field, are shifted about 0.1 eV downwards to lower energy. This shift can be explained by an extensive hybridization with the lower-lying Cu d_{z^2} orbital. This is in contrast to the band structure of thermoelectric material Na_xCoO_2, where the band crossing Fermi level has the a_{1g} character.

In the LDA+U calculation, the gap is increased to 1.6 eV for the chosen value $U = 2.7$ eV. The most prominent change in comparison with the LDA could be found within 0.5 eV below E_F. The total DOS is about twice reduced within this range, and Co d states are almost completely suppressed and replaced by Cu d states, predominantly of d_{z^2} symmetry. However, since this electron transfer is only realized below the Fermi level, the occupation of transition-metal d orbitals remains similar to the LDA calculation.

Let us discuss in more detail the difference in the orbital's character at the Fermi level between the LDA and LDA+U calculations. The octahedral crystal field splits the Co d orbitals into e_g orbitals directed to oxygens and t_{2g} orbitals. The trigonal field, which lifts the degeneracy of t_{2g} orbitals, is much smaller than the t_{2g} bandwidth and will be neglected in the following discussion. A smaller Co-O-Co bond angle (of less than 180°) decreases the hybridization, narrows the Co d-O p bands, and favors the crystal-field splitting in the competition with the bandwidth and thus supports the LS state of Co^{3+} (t^6_{2g} e^0_g) [30]. Since the Co-O-Co bond angle in delafossite is close to 90°, higher spin states are shifted to high energy and are very unlikely compared to perovskites, where spin transitions may be induced by increasing temperature. Therefore, the Co states at Fermi level in $CuCoO_2$ are the narrow t_{2g} bands, whereas the broad Co e_g bands are high above the E_F. As regards Cu with d^{10} orbital occupation, the Cu states at E_F are the broad a_{1g} bands formed by orbitals pointing towards bonding oxygens. It was evidenced in the study of transition-metal perovskites that the impact of U is generally bigger on the narrow (t_{2g}) bands than on the broad (e_g) bands [31]. In accordance, in our case of $CuCoO_2$, the influence of U is bigger on more narrow Co t_{2g} orbitals, which are shifted down below the Fermi level, than on broader Cu d_{z^2}, which are less affected and replace the Co orbitals at E_F.

Taking into consideration that octahedrally coordinated Fe^{3+} (d^5 configuration) occurs in oxides, including $CuFeO_2$ [19,32], always in a high-spin (HS) state, we have to realize that it is not possible to use a virtual atom simulation of Fe for Co substitution in $CuCoO_2$ since the VA approximation assumes compatible configuration of the valence electrons and cannot simulate the LS state of Co^{3+} and the HS state of Fe^{3+}

at the same time. The trial LDA+U calculation revealed that indeed the LS state of the virtual atom $Co_{1-x}Fe_x$ is more stable for $x < 0.5$ and the HS state has lower energy for $x > 0.5$, reaching the expected magnetic moment 5 μ_B *per* formula unit for $CuFeO_2$. But these results should only be considered as an artifact of the VA approximation and will not be used for further calculations. Moreover, in the LDA calculation, the LS state is more stable for the whole x range including $CuFeO_2$, so using the LDA+U method for a correct description of the Fe configuration is necessary in this case.

The Ni^{3+} cation octahedrally coordinated by oxygen is typically in a LS state, so the virtual atom approximation is valid for the simulation of electron doping into the CoO_2 layer by substitution of Ni for Co. The DOS of $CuCo_{1-x}Ni_xO_2$ modeled by the VA approximation is shown for $x = 0.2$ in Fig. 3. The electrons are doped both into Co e'_g and e_g orbitals, whereas occupation of the Co a_{1g} band remains constant. The calculated DOS is nonmagnetic close to $x = 0$ and the magnetic moment appears from $x = 0.5$ for the LDA and $x = 0.2$ for the LDA+U calculation.

The hole doping into the Cu layer was similarly simulated by substitution of Ni for Cu using the VA approximation.

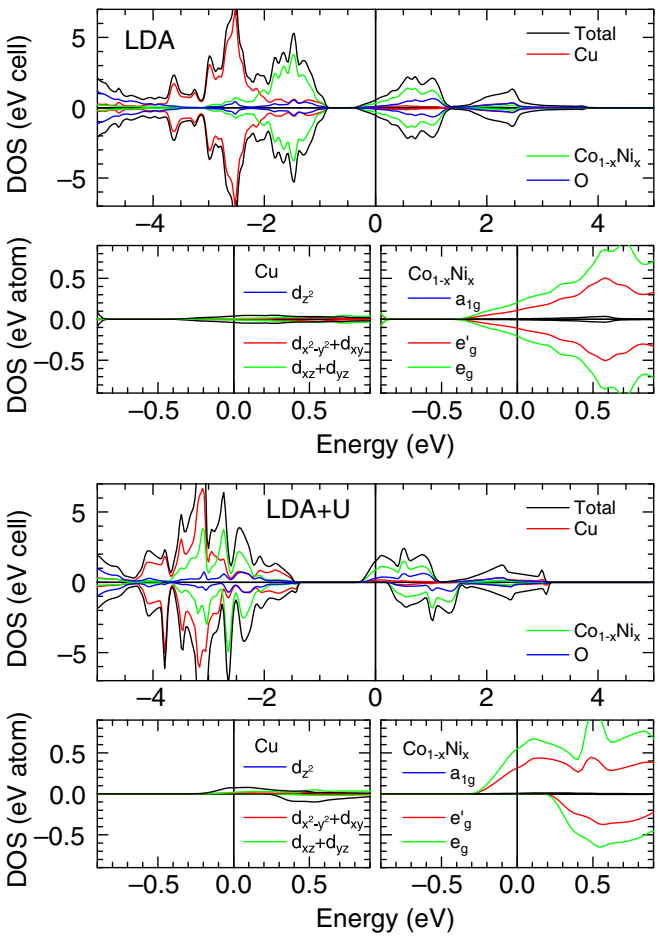

FIG. 3. (Color online) LDA (upper panels) and LDA+U (lower panels) density of states, and projections of Cu and virtual atom $Co_{1-x}Ni_x$ d orbitals onto LAPW spheres, obtained using the VA approximation for $CuCo_{1-x}Ni_xO_2$ with $x = 0.2$. The total DOS is *per* primitive unit cell, and the partial DOS is *per* atom.

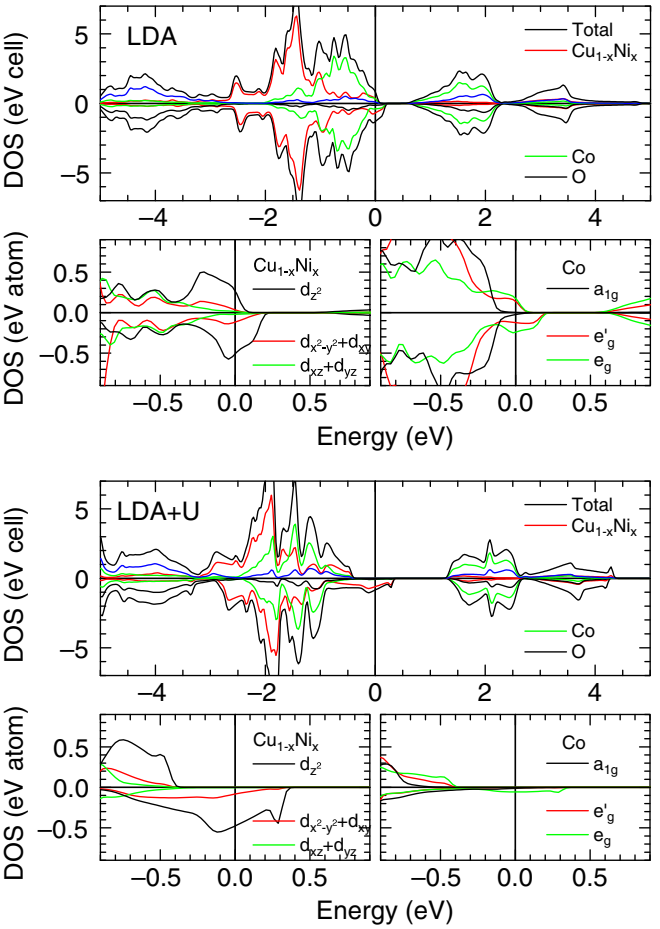

FIG. 4. (Color online) LDA (upper panels) and LDA+U (lower panels) density of states, and projections of virtual atom $Cu_{1-x}Ni_x$ and Co d orbitals onto LAPW spheres, obtained using the VA approximation for $Cu_{1-x}Ni_xCoO_2$ with $x = 0.2$. The total DOS is *per* primitive unit cell, and the partial DOS is *per* atom.

Electronic configurations of Cu^{1+} (d^{10}) and Ni^{1+} (d^9) are compatible as regards the VA approximation. But we have to consider that Ni^{1+} is not a typical valence state and the Ni cation does not usually accept linear coordination, so the actual substitution should be realized with Pd rather than Ni.

The DOS of $Cu_{1-x}Ni_xCoO_2$ calculated using the VA approximation is displayed for $x = 0.2$ in Fig. 4. The orbital projection of DOS reveals that the holes are doped mainly into the Cu d_{z^2} orbital and less to the Co e'_g and e_g orbitals for the LDA calculation. In the LDA+U calculation, the Co d orbitals are pushed below E_F and the Fermi level is dominated just by the spin-down Cu d_{z^2} orbital. In spite of the mixed character of the orbitals near the Fermi level, the occupation is only changed in the Cu d_{z^2} orbital both for LDA and LDA+U.

Let us note, for the sake of comparison with the results of the rigid band approximation in Ref. [6], that the rigid band approximation does not actually distinguish among doping at various sites, i.e., between substitution at a Co or Cu site in our case.

The DOS of $CuCo_{1-x}Fe_xO_2$ obtained by the LDA+U supercell calculation is shown for $x = 2/12$ in Fig. 5. The DOS is characterized by a gap of about 1.5 eV. The states

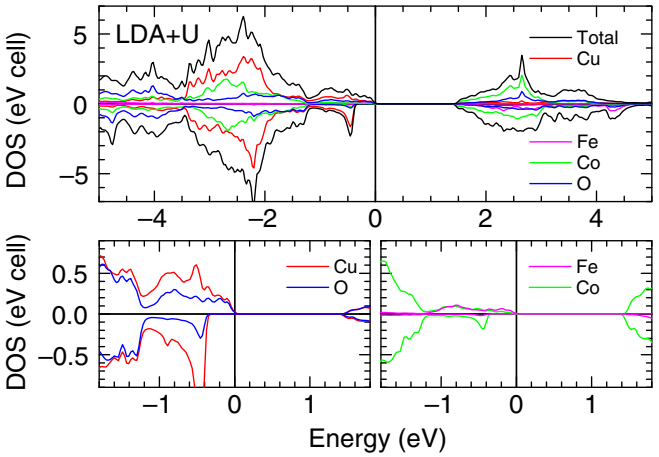

FIG. 5. (Color online) LDA+U density of states obtained by supercell calculation for $CuCo_{1-x}Fe_xO_2$ with $x = 2/12$. The absolute value of the DOS was scaled to the primitive unit-cell volume for comparison with the VA calculation.

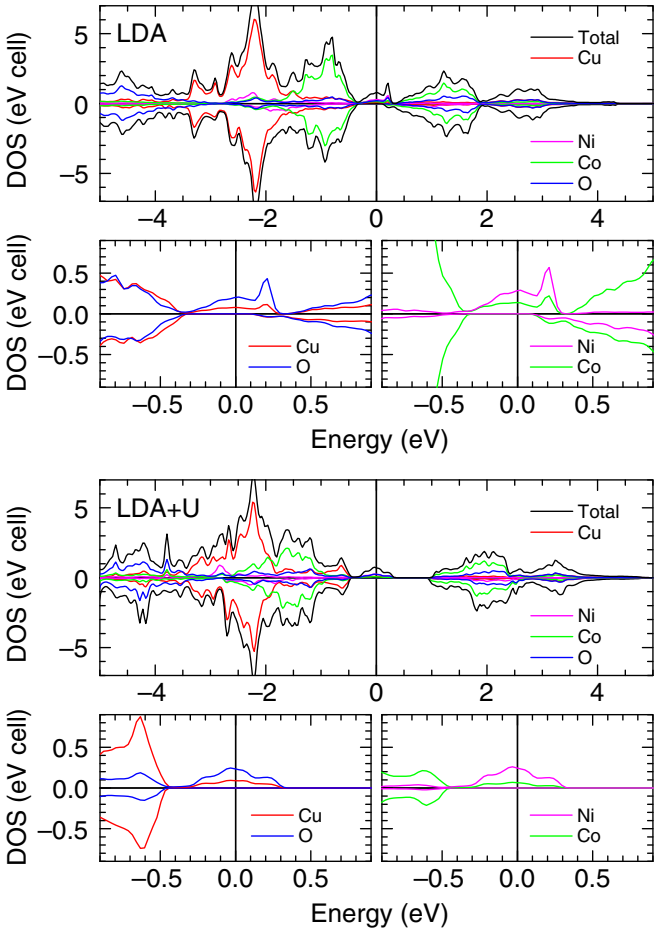

FIG. 6. (Color online) LDA (upper panels) and LDA+U (lower panels) density of states obtained by supercell calculation for $CuCo_{1-x}Ni_xO_2$ with $x = 2/12$. The absolute value of the DOS was scaled to the primitive unit-cell volume for comparison with the VA calculation.

below the Fermi level are formed mainly by Cu and O with a small contribution of Fe spin-up bands. The resulting magnetic moment corresponds to the number of doped iron atoms, i.e., 5 μ_B *per* Fe.

The DOS of $CuCo_{1-x}Ni_xO_2$ obtained by the supercell calculation is displayed for $x = 2/12$ in Fig. 6. The electron doping creates new states ± 0.3 eV around the Fermi level that fill the gap in the spin-up channel. These states are formed mainly by Ni and O. The rest of the DOS is almost unchanged compared to $CuCoO_2$.

The DOS of $Cu_{1-x}Pd_xCoO_2$ obtained by the supercell calculation is illustrated for $x = 2/12$ in Fig. 7. Doping of Pd for Cu pushes Co bands down in energy about 0.2 eV away from the Fermi level, leaving a small density of states of ± 0.2 eV around E_F, contributed by all kinds of atoms with a prevalence of Pd and Cu. The resulting DOS is nonmagnetic for the LDA calculation. The inclusion of correlation effects in the LDA+U calculation has the following effects. The Pd projected DOS is enhanced over that of Co. Spin-up states are shifted to lower energy, resulting in a magnetic moment of about 0.6 μ_B *per* doped Pd.

The transport properties were calculated within standard Boltzmann theory. Assuming the constant scattering time approximation, the thermopower $S(T)$ can be obtained from the band structure within Boltzmann transport formalism with no need for adjustable parameters. This approximation involves the assumption that the energy dependence in the Boltzmann transport equations is dominated by the energy dependence of the band structure and not the scattering time within a few kT around E_F [14]. The formula used in the calculation has a general form,

$$S_{ij} = \frac{1}{eT} K^1_{\alpha j}/K^0_{\alpha i}, \tag{1}$$

where $K^n_{\alpha\beta}(T,\mu)$ is

$$K^n_{\alpha\beta} = \int \frac{\tau_\epsilon(\epsilon-\mu)^n}{\hbar^2} \frac{\partial\epsilon}{\partial \mathbf{k}_\alpha} \frac{\partial\epsilon}{\partial \mathbf{k}_\beta} \left[-\frac{\partial f_\mu(T,\epsilon)}{\partial\epsilon}\right] d\epsilon, \tag{2}$$

where μ is the chemical potential, ϵ is an energy variable, T is the absolute temperature, e is the electron charge, and τ is a relaxation time. The main weight in the above-mentioned integration has partially occupied states at characteristic energy $\mu \pm 3kT$, which is approximately ± 75 eV around the chemical potential at 300 K and approx. ± 200 eV at 800 K.

Thermopower calculated for $CuCo_{1-x}Ni_xO_2$ and $Cu_{1-x}Ni_xCoO_2$ using the band structure obtained by the virtual atom approximation is displayed for the LDA calculation in Fig. 8 and for the LDA+U calculation in Fig. 9. As expected, the Seebeck coefficient is positive for the hole-doping case $Cu_{1-x}Ni_xCoO_2$ and negative for the electron-doping case $CuCo_{1-x}Ni_xO_2$.

Let us compare the thermopower of $CuCo_{1-x}Ni_xO_2$ from the LDA calculations using the VA approximation with the results of electron doping by the rigid band approximations in Ref. [6]. Since the doping ranges are different in these works, only the $x = 0.1$ doping level may directly be compared. It is seen that the calculated thermopower at 800 K is about -100 μV/K in both cases, so the virtual atom and rigid band approximations gave comparable results. The calculated thermopower obtained from LDA+U is basically the same

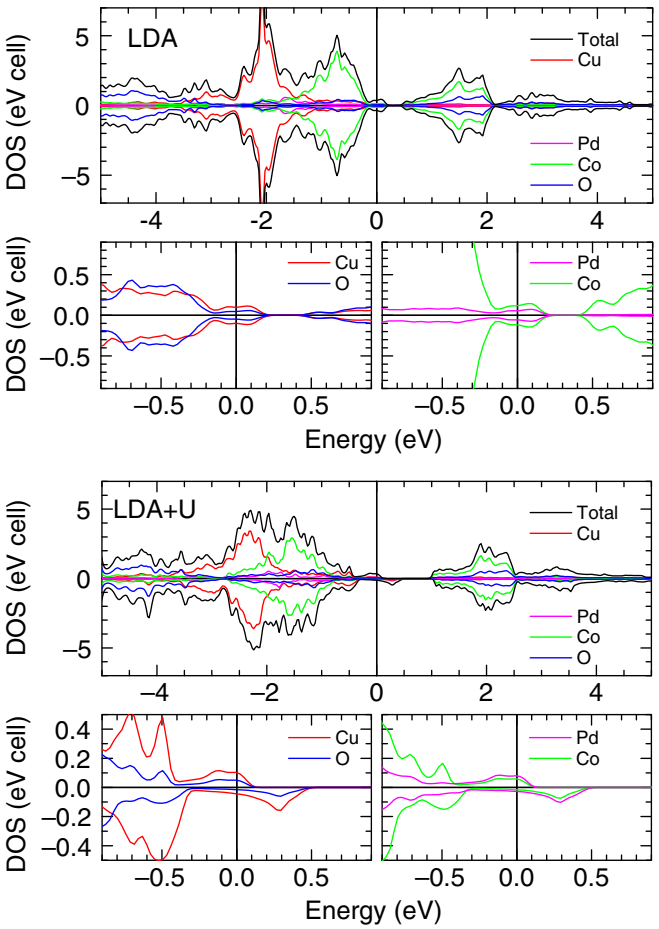

FIG. 7. (Color online) The LDA (upper panels) and LDA+U (lower panels) density of states obtained by the supercell calculation for $Cu_{1-x}Pd_xCoO_2$ with $x = 2/12$. The absolute value of the DOS was scaled to the primitive unit-cell volume for comparison with the VA calculation.

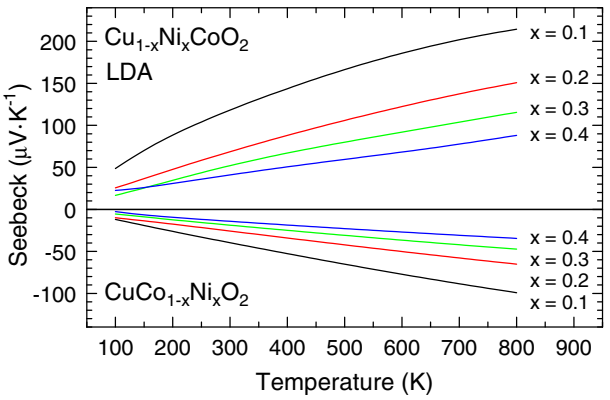

FIG. 8. (Color online) Calculated thermopower based on valence-band dispersion obtained in the LDA calculation with the VA approximation for $CuCo_{1-x}Ni_xO_2$ and $Cu_{1-x}Ni_xCoO_2$. $x = 0.1$ (black line), $x = 0.2$ (red line), $x = 0.3$ (green line), and $x = 0.4$ (blue line).

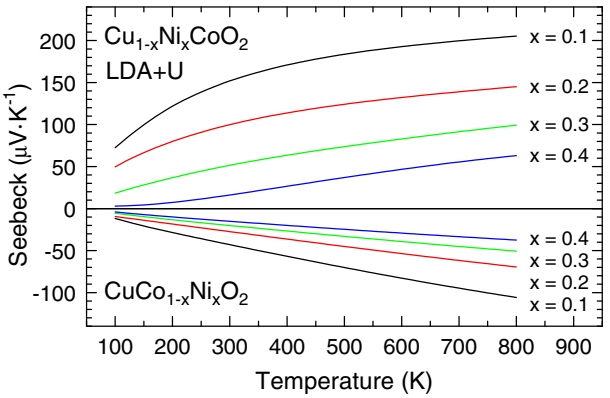

FIG. 9. (Color online) Calculated thermopower based on valence-band dispersion obtained in the LDA+U calculation with the VA approximation for $CuCo_{1-x}Ni_xO_2$ and $Cu_{1-x}Ni_xCoO_2$. Line colors as in Fig. 8.

as that from LDA. The DOS around E_F is polarized in the LDA+U calculation, so that there is only spin-up DOS over the range ± 0.2 eV around the Fermi level. But the shape of the spin-up DOS of LDA+U is practically the same as the sum of the spin up and down of LDA, thus also the resulting thermopower is practically the same.

The thermopower of $Cu_{1-x}Ni_xCoO_2$ from the LDA calculation using the VA approximation could be compared with hole doping by the rigid band approximations in Ref. [6]. If we compare $x = 0.1$ and 0.2 doping levels, we can see that the values of thermopower at 800 K are quite similar, i.e., the thermopower obtained in our calculation is only about 10% lower. The thermopower from the LDA+U calculation is different at lower temperatures, whereas at high temperatures, the results of LDA and LDA+U are almost identical. Similarly as in the $CuCo_{1-x}Ni_xO_2$ case, including LDA+U increased the DOS polarization around E_F, but the shape of the spin-up

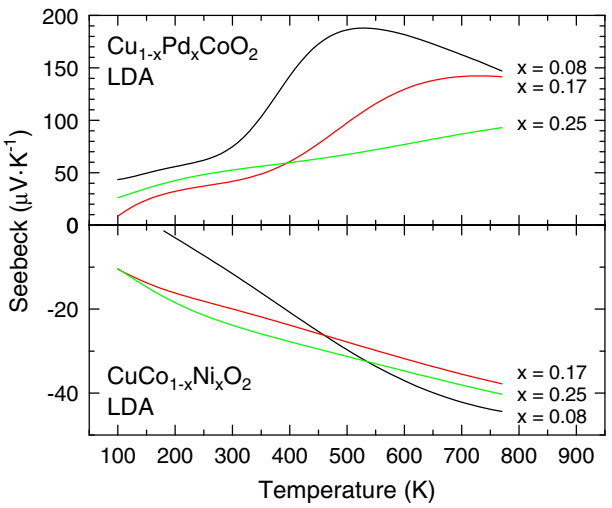

FIG. 10. (Color online) Calculated thermopower based on valence-band dispersion obtained in the LDA calculation with the supercell approximation for $CuCo_{1-x}Ni_xO_2$ and $Cu_{1-x}Pd_xCoO_2$. $x = 1/12$ (black line), $x = 2/12$ (red line), and $x = 3/12$ (green line).

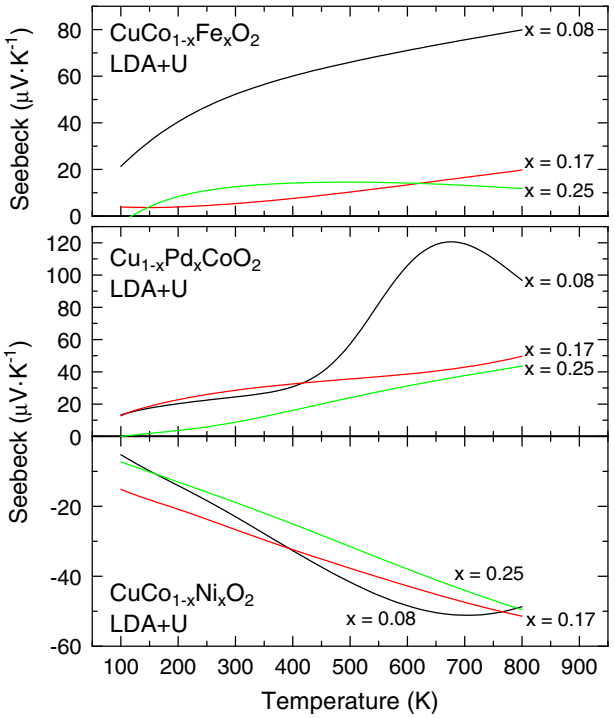

FIG. 11. (Color online) Calculated thermopower based on valence-band dispersion obtained in the LDA+U calculation with the supercell approximation for $CuCo_{1-x}Fe_xO_2$, $CuCo_{1-x}Ni_xO_2$, and $Cu_{1-x}Pd_xCoO_2$. Line colors as in Fig. 10.

DOS is again practically the same as the sum of the spin up and down of LDA. Nevertheless, small changes in the DOS shape around the Fermi level are reflected at low T, but they are smeared out at high T where the thermopower is calculated from a wider range of energy.

Thermopower calculated for $CuCo_{1-x}Ni_xO_2$ and $Cu_{1-x}Pd_xCoO_2$ using the band structure obtained by the supercell calculation is displayed for the LDA calculation in Fig. 10 and for the LDA+U calculation including $CuCo_{1-x}Fe_xO_2$ in Fig. 11.

The thermopower of the supercell calculation is mostly reduced compared to the VA approximation, especially in the case of hole-doped LDA+U thermopower. This is because in the supercell calculation a low and dispersed DOS is typically formed around E_F, while the narrow and high DOS, which is favorable for getting high thermopower, is pushed down below the Fermi level. This effect is more pronounced in the LDA+U calculation, since the impact of U on the narrow bands is higher than on the broad bands, as discussed above.

This behavior reflects the basic difference between Na_xCoO_2 and doped $CuCoO_2$. In Na_xCoO_2, the doping is achieved by variation of Na^+ stoichiometry, and since the bonding of Na to oxygen has an ionic character and the electronic states of Na are far below the Fermi level, the doping does not alter the band structure around E_F and the rigid band approximation is valid. In $CuCoO_2$, owing to the similar energy of Co and Cu d orbitals and hybridization of symmetrically related Co a_{1g} and Cu d_{z^2}, both cations contribute significantly to the bands around the Fermi level. Therefore, substitution at any of the cation sites alters the band structure at E_F and affects the thermoelectric properties.

IV. CONCLUSIONS

The evolution of the band structure and thermoelectric properties of $CuCoO_2$ upon hole and electron doping at the Co site and hole doping at the Cu site were calculated by the LDA and LDA+U methods. The doping was simulated by the virtual atom approximation and the supercell approach and the results were compared with previous calculations using the rigid band approximation [6].

The band structure of $CuCoO_2$ is influenced by the hybridization between symmetrically related Co a_{1g} and Cu d_{z^2} orbitals, which pushes the Co a_{1g} orbital down below the Fermi level, so that bands at E_F have the Co e_g' and e_g character. This is in contrast to the band structure of thermoelectric material Na_xCoO_2, where the band crossing Fermi level has the a_{1g} character, in accordance with one-electron levels splitting in the crystal field of trigonal coordination compressed along the z axis.

The calculated thermopower within standard Boltzmann theory is comparable for the virtual atom and rigid band approximations. However, the thermopower based on the supercell calculation is significantly lower. This is because in the supercell calculation a low and dispersed DOS is formed around E_F, while the narrow and high DOS, which is favorable for getting high thermopower, is pushed down below the Fermi level. This effect is more pronounced in LDA+U calculations, since the impact of U on the narrow bands is higher than on the broad bands. Whereas the rigid band approximation does not distinguish among doping at various sites, our results show that in the case of hole doping, higher thermopower is obtained for substitution at the Cu site than in the CoO_2 layer.

ACKNOWLEDGMENTS

This work was supported by Project No. 13-03708S of the Grant Agency of the Czech Republic.

[1] I. Terasaki, Y. Sasago, and K. Uchinokura, Phys. Rev. B **56**, R12685 (1997).
[2] Y. Wang, N. S. Rogado, R. J. Cava, and N. P. Ong, Nature (London) **423**, 425 (2003).
[3] M. Lee, L. Viciu, L. Li, Y. Wang, M. L. Foo, S. Watauchi, R. A. Pascal, R. J. Cava, and N. P. Ong, Nat. Mater. **5**, 537 (2006).
[4] J. W. Fergus, J. Eur. Ceram. Soc. **32**, 525 (2012).
[5] D. Vengust, B. Jancar, A. Sestan, M. P. Svet, B. Budic, and D. Suvorov, Chem. Mater. **25**, 4791 (2013).
[6] D. J. Singh, Phys. Rev. B **76**, 085110 (2007).
[7] E. F. Bertaut and C. Delorme, C. R. Acad. Sci., Paris **238**, 1829 (1954).
[8] R. D. Shannon, D. B. Rogers, and C. T. Prewitt, Inorg. Chem. **10**, 713 (1971).

[9] J. P. Doumerc, A. Wichainchai, A. Ammar, M. Pouchardand, and P. Hagenmuller, Mater. Res. Bull. **21**, 745 (1986).
[10] M. Beekman, J. Salvador, X. Shi, G. S. Nolas, and J. Yang, J. Alloys Compd. **489**, 336 (2010).
[11] H. H. Emons and E. Beger, Z. Chem. **7**, 200 (1967).
[12] P. Porta, R. Dragone, G. Fierro, M. Inversi, M. L. Jacono, and G. Moretti, J. Chem. Soc. Faraday Trans. **88**, 311 (1992).
[13] W. C. Sheets, E. Mugnier, A. Barnabe, T. J. Marks, and K. R. Poeppelmeier, Chem. Mater. **18**, 7 (2006).
[14] G. K. H. Madsen and D. J. Singh, Comput. Phys. Commun. **175**, 67 (2006).
[15] C. T. Prewitt, R. D. Shannon, and D. B. Rogers, Inorg. Chem. **10**, 719 (1971).
[16] M. Mekata, N. Yaguchi, T. Takagi, T. Sugino, S. Mitsuda, H. Yoshizawa, N. Hosoito, and T. Shinjo, J. Phys. Soc. Jpn. **62**, 4474 (1993).
[17] K. Hayashi, T. Nozaki, and T. Kajitani, Jpn. J. Appl. Phys. **46**, 5226 (2007).
[18] M. Uhrmacher, R. N. Attili, K. P. Lieb, K. Winzer, and M. Mekata, Phys. Rev. Lett. **76**, 4829 (1996).
[19] F. Ye, J. A. Fernandez-Baca, R. S. Fishman, Y. Ren, H. J. Kang, Y. Qiu, and T. Kimura, Phys. Rev. Lett. **99**, 157201 (2007).
[20] K. El Ataoui, A. Ammar, J. P. Doumerc, J. C. Grenier, P. Dordor, and M. Pouchard, C. R. Chimie **7**, 29 (2004).
[21] M. Tanaka, M. Hasegawa, and H. Takei, J. Phys. Soc. Jpn. **65**, 3973 (1996).
[22] M. Hasegawa, I. Inagawa, M. Tanaka, I. Shirotani, and H. Takei, Solid State Commun. **121**, 203 (2002).
[23] K. P. Ong, J. Zhang, J. S. Tse, and P. Wu, Phys. Rev. B **81**, 115120 (2010).
[24] K. P. Ong, D. J. Singh, and P. Wu, Phys. Rev. Lett. **104**, 176601 (2010).
[25] P. Blaha, K. Schwarz, G. K. H. Madsen, D. Kvasnicka, and J. Luitz, *WIEN2k, An Augmented Plane Wave + Local Orbitals Program for Calculating Crystal Properties* (Technische Universität, Wien, 2001).
[26] K. Knížek, Z. Jirák, J. Hejtmánek, and P. Novák, J. Phys. Condens. Matter **18**, 3285 (2006).
[27] K. Knížek, Z. Jirák, J. Hejtmánek, P. Novák, and W. Ku, Phys. Rev. B **79**, 014430 (2009).
[28] R. F. W. Bader, *Atoms in Molecules-A Quantum Theory* (Oxford University Press, Oxford, 1990).
[29] K. Knížek, J. Hejtmánek, P. Novák, and Z. Jirák, Phys. Rev. B **81**, 155113 (2010).
[30] K. Knížek, P. Novák, and Z. Jirák, Phys. Rev. B **71**, 054420 (2005).
[31] I. Solovyev, N. Hamada, and K. Terakura, Phys. Rev. B **53**, 7158 (1996).
[32] T. Nakajima, A. Suno, S. Mitsuda, N. Terada, S. Kimura, K. Kaneko, and H. Yamauchi, Phys. Rev. B **84**, 184401 (2011).